THE JOURNAL OF PHYSICAL CHEMISTRY B

ARTICLE

pubs.acs.org/JPCB

Correlation between Crystallization Kinetics and Electroactive Polymer Phase Nucleation in Ferrite/Poly(vinylidene fluoride) Magnetoelectric Nanocomposites

P. Martins, C. M. Costa, J. C. C. Ferreira, and S. Lanceros-Mendez*

Centro/Departamento de Física da Universidade do Minho, 4710-057 Braga, Portugal

ABSTRACT: Poly(vinylidene fluoride) (PVDF) nanocomposites with different ferrite nanoparticle loadings are interesting as, depending on ferrite type and content, the electroactive β-phase of the polymer is nucleated and the magnetoelectric coupling is induced. The isothermal crystallization behavior of ferrite/PVDF nanocomposites is studied using polarized optical microscopy, and the crystallization kinetic is analyzed by the Avrami theory in order to understand the crystallization conditions leading to the nucleation of the electroactive polymer phase. It is found that the nucleation kinetics is enhanced by the presence of ferrite nanoparticles, as evidenced by the increasing number of spherulites with increasing nanoparticle content and by the variations of the Avrami exponent. The crystallization velocity is intimately related to the polymer α- or β-phase formation in the nanocomposites and follows the order $NiFe_2O_4$/PVDF > $CoFe_2O_4$/PVDF > $Ni_{0.5}Zn_{0.5}Fe_2O_4$/PVDF for a given temperature and nanoparticle loading, which results in larger amounts of β-phase for $CoFe_2O_4$/PVDF and $Ni_{0.5}Zn_{0.5}Fe_2O_4$/PVDF nanocomposites.

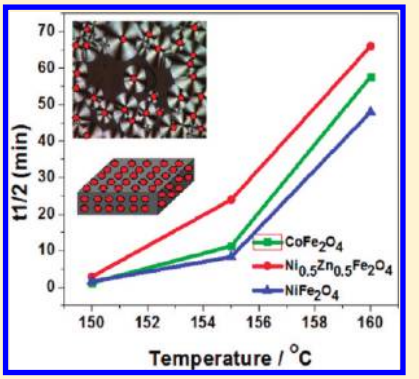

INTRODUCTION

Polyvinylidene fluoride (PVDF) and its composites are intensively studied due to their excellent piezoelectric, pyroelectric, and ferroelectric properties.[1−3]These properties combined with high elasticity and easy processability make this material interesting for numerous technological applications.[4]

Also interesting in this polymer is its polymorphism, showing four different crystalline forms, named α, β, δ, and γ, which appear depending on the processing conditions.[5] The α- and β-phases are the most studied polymorphs. The nonpolar α-phase is the most common one as it is obtained when the polymer is cooled from the melt at moderated or high cooling rates and therefore is the one readily obtained in conventional processing polymer methods such as extrusion.[6−8]

The ferroelectric β-phase has a nonzero dipole moment and is widely used in technological applications such as sensors, actuators, batteries, and membranes due to its exceptional electroactive properties among polymer materials.[9−11] β-PVDF is usually obtained by stretching α-phase films at stretch ratios from 3 to 5 at controlled temperature between 70 and 100 °C.[15]

β-phase samples can also be obtained by solvent casting methods when the material is crystallized at temperatures below 70 °C, but the samples reveal high porosity,[7] showing, therefore, poor mechanical and electrical properties and compromising the applicability of these materials.[12−14]

Consequently, strong efforts are being undertaken to develop easy to process, stable, and nonporous β-PVDF. Some examples of these approaches are the crystallization under high pressure, the use of copolymers such as poly(vinylidene trifluorethylene) (P(VDF-TrFE)), or the incorporation of nanoclays into PVDF.[16−18]

A more recent and interesting approach is the nucleation of the electroactive phase of the polymer by the incorporation of ferrite nanoparticles into PVDF.[19,20] Ferrite nanoparticles are usually used as the magnetostrictive phase in magnetoelectric composites and are interesting both for fundamental studies and technological applications.[20,21] In this case, nanoparticles can be used both for inducing the electroctive phase of the polymer, when low particle loadings are used, or for the preparation of magnetoelectric materials, for higher nanoparticle contents.[20,22] In this way, the physical properties of PVDF depend not only upon the processing conditions but are also strongly influenced by the presence of such nanoparticles. The presence of the nanoparticles can determine the crystallized phase and the resulting polymer microstructure and morphology[23] through variations, among other effects, in the crystallization kinetics.[24] In this way, it also interesting to study the influence of the nanoparticles in the crystallization kinetics both in order to study the interactions responsible for the variations in the crystallization kinetics and also in order to study the origin of the β-phase nucleation.[25−29]

The influence of ferrite nanoparticles in the polymer crystallization kinetics has been previously addressed by measuring the crystallization kinetics of composites by means of isothermal experiments and cooling scans using differential scanning calorimetry.[30,31] It was concluded that the nucleation kinetics is enhanced by the presence of nanoparticles, as corroborated by the

Received: November 1, 2011
Revised: December 10, 2011
Published: December 15, 2011

increasing number of spherulites and variations of the Avrami's exponent with increasing nanoparticle content.[32] Nevertheless, for further understand of the nucleation effect, the variations in the crystallization kinetics is investigated in the present work by polarized optical microscopy in three different ferrites, $CoFe_2O_4$, $NiFe_2O_4$, and $Ni_{0.5}Zn_{0.5}Fe_2O_4$, with different electroactive phase nucleation ability and analyzing spherulite and microstructure evolution over ferrite type, concentration, and crystallization temperature.

The different ferrites were chosen as, together with being all suitable for the development of ME materials, all of them have the ability to fully nucleate the β-phase of PVDF but with different concentration dependence, allowing, therefore, a complete study, understanding, and control of the relationship between the PVDF β-phase nucleation process and the polymer crystallization kinetics.

CRYSTALLIZATION KINETICS

The isothermal crystallization kinetics of polymers is commonly analyzed within the Avrami theory, as represented by eq 1,[33,34]

$$1 - X_t = \exp(-Kt^n) \quad (1)$$

where n is the Avrami exponent, which depends on the nature of the nucleation and growth geometry of the crystals, K is a rate constant involving both nucleation and growth rate parameters, X_t is the relative crystallinity, and t is the crystallization time. Equation 1 can be applied only when the nucleation and growth conditions do not change during the crystallization.[32,33]

From images like the ones presented in Figure 1, obtained by polarized optical microscopy at regular time intervals during the crystallization process time, t, evolution of the fraction (X_t) of the material that crystallizes can be calculated from the evolution of the crystallized area as a function of time $(\partial A/\partial t)$

$$X_t = \frac{\int_0^t (\partial A/\partial t)\partial t}{\int_0^\infty (\partial A/\partial t)\partial t} \quad (2)$$

where the numerator represents the crystallized area at a given time, and the denominator is the total area of the fully crystallized material.[35]

The crystallization half-time, $t_{1/2}$, defined as the time at which the extent of crystallization is 50%, can be obtained from eq 3,[32]

$$t_{1/2} = \left(\frac{\ln 2}{K}\right)^{1/n} \quad (3)$$

Finally, the activation energy of the crystallization process is obtained by applying the Arrhenius equation to the overall crystallization rate constant K, containing contributions from both nucleation and growth rate,[35]

$$K = A^{(-E_{act}/RT_{crystallization})} \quad (4)$$

where A is the pre-exponential factor, E_{act} is the activation energy of the crystallization process, and R is the ideal gas constant (R = 8.31 J mol^{-1} K^{-1}).[36,37]

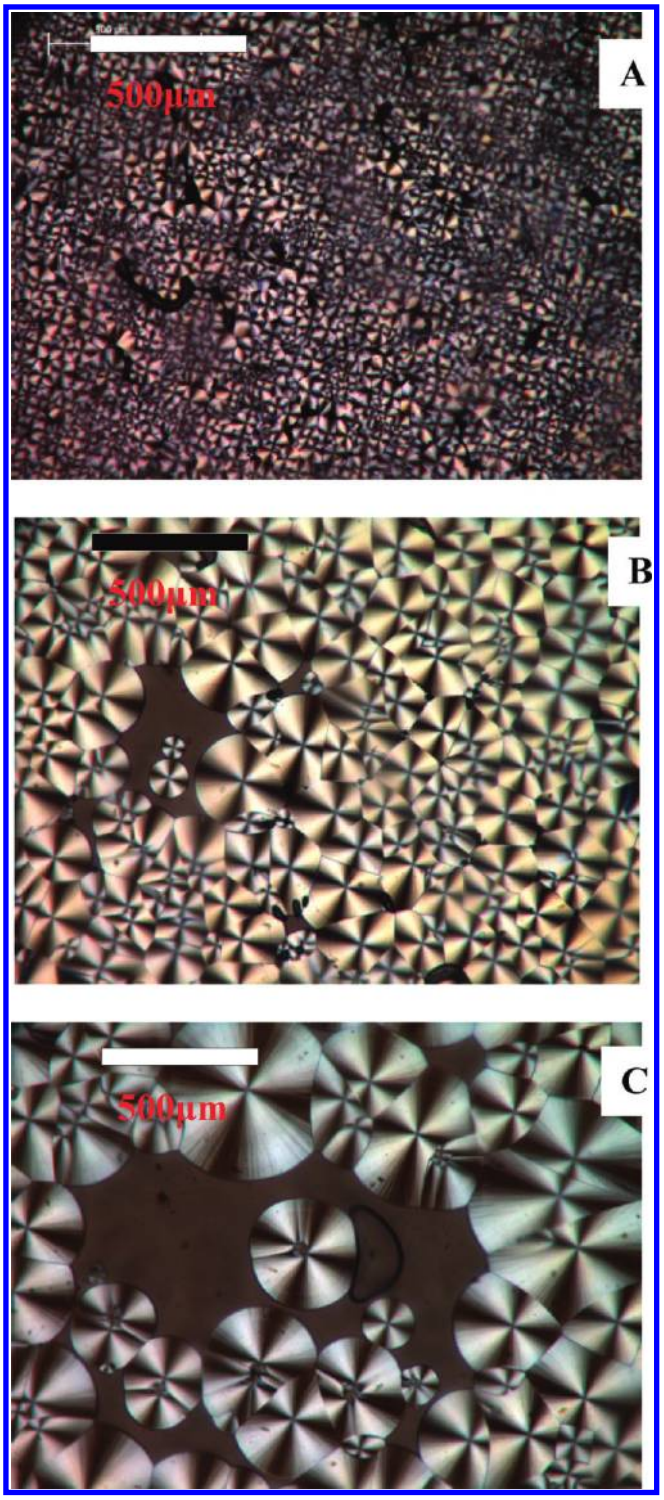

Figure 1. Images of spherulitic growth for the $CoFe_2O_4$/PVDF composite with 0.01 wt % ferrite with 5200 s crystallization time at (A) 150, (B) 155, and (C) 160 °C.

EXPERIMENTAL SECTION

$CoFe_2O_4$, $NiFe_2O_4$, and $Ni_{0.5}Zn_{0.5}Fe_2O_4$ nanoparticles were purchased from Nanoamor, having dimensions between 35−55, 20−30, and 10−30 nm, respectively.[38] *N*,*N*-dimethylformamide (DMF, pure grade) was obtained from Fluka, and poly(vinilidene

dx.doi.org/10.1021/jp210493t |J. Phys. Chem. B 2012, 116, 794–801

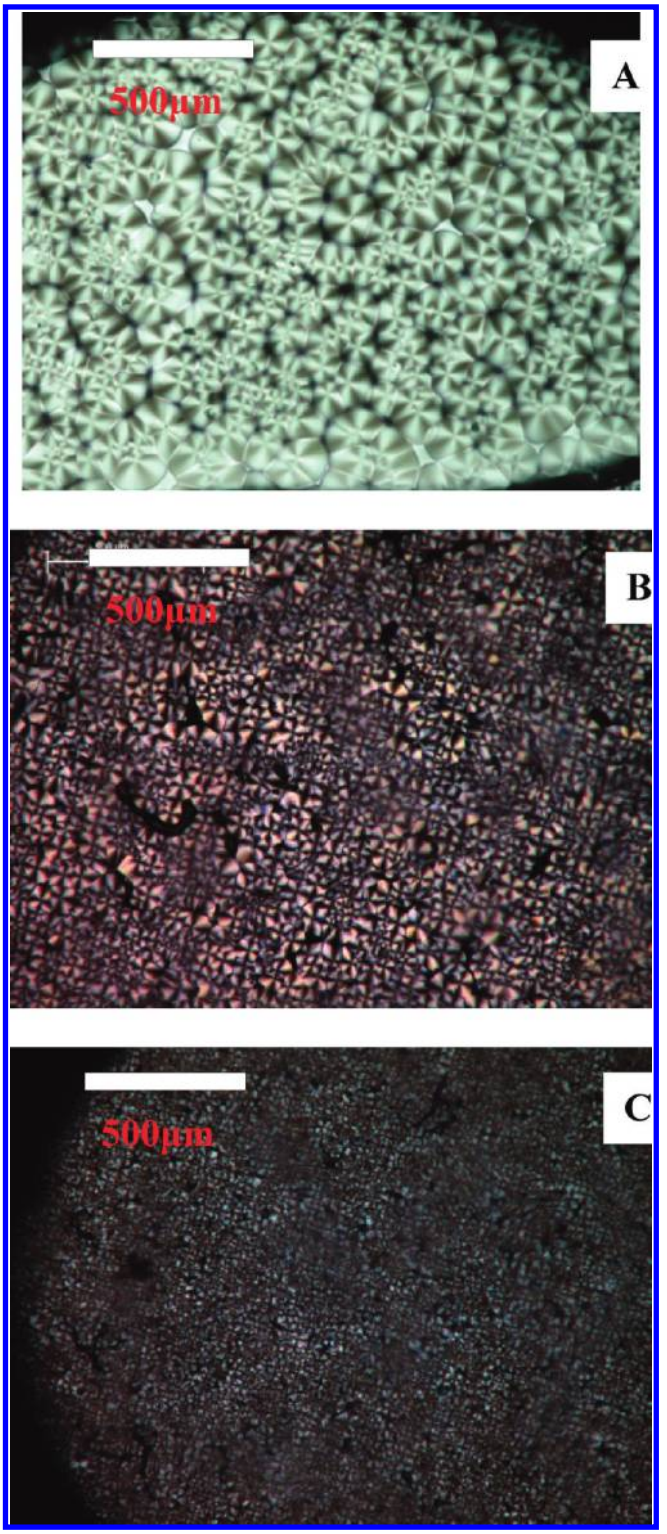

Figure 2. Images of spherulitic growth for the $CoFe_2O_4$/PVDF nanocomposite ferrite with 5200 s crystallization time at 150 °C with $CoFe_2O_4$ wt % (A) 0, (B) 0.01, and (C) 1.

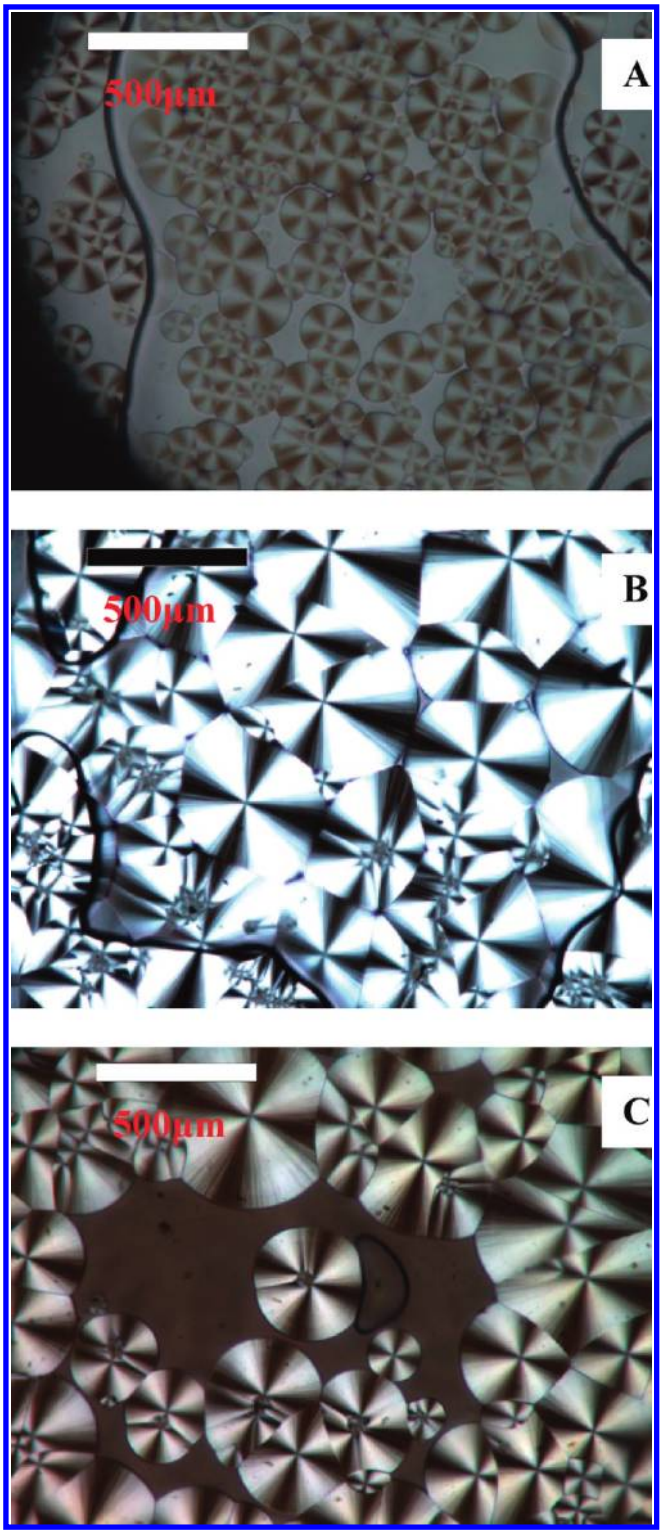

Figure 3. Images of spherulitic growth for the ferrite/PVDF (0.01 wt %) samples crystallized at 160 °C with 5200 s crystallization time: (A) $Ni_{0.5}Zn_{0.5}Fe_2O_4$, (B) $NiFe_2O_4$, and (C) $CoFe_2O_4$ nanoparticles.

fluoride) (PVDF, Solef 1010) powder was supplied by Solvay. All the chemicals and nanoparticles were used as received from the suppliers. For the preparation of the films, the initial concentration of the solution was 0.2 g of PVDF for 1 mL of DMF. Then, the multiferroic nanocomposites were prepared by adding the desired amount of nanoparticles to 12 mL of DMF and placing them in an ultrasound bath for 6 h to ensure that the nanoparticles were well dispersed in the solution and to avoid aggregates. Then, PVDF was added. The weight percentage (wt %) of the ferrite

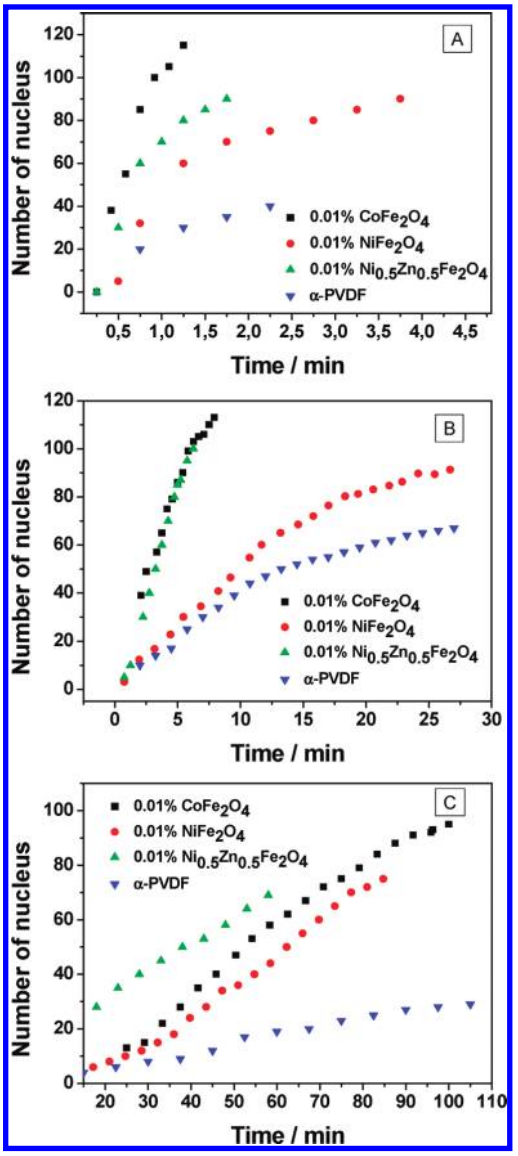

Figure 4. Number of nuclei over time to ferrite/PVDF (0.01 wt %) samples crystallized at (a) 150, (b) 155, and (c) 160 °C.

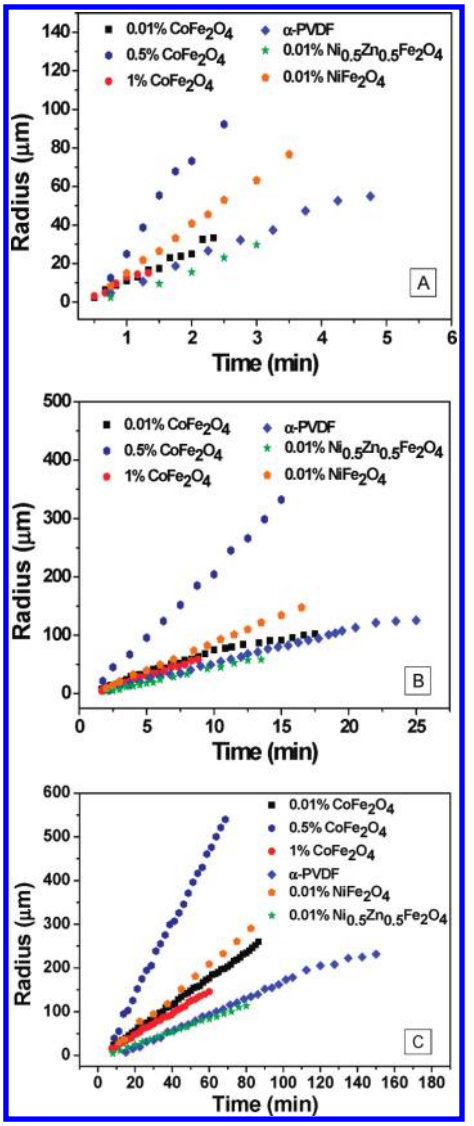

Figure 5. Spherulitic growth of the different nancomposites with crystallization temperatures (A) 150, (B) 155, and (C) 160 °C.

nanoparticles was varied from 0.001% to 50% corresponding to a 3 $\times$ 10^{-6} to 0.25 volume fraction.

The mixture was then placed in a Teflon mechanical stirrer for complete dissolution of the polymer, and flexible films of $\sim$50 μm were obtained by spreading the solution on a clean glass substrate. Solvent evaporation and polymer melting were obtained inside an oven at a controlled temperature of 210 °C for 10 min. After this process, samples were crystallized by cooling down to room temperature.

Images of spherulitic growth during the crystallization of the PVDF nanocomposites were obtained by an optical microscope with polarized light (Leica DM 2500M) provided with a Leica DFC-295 camera. The hot plate used was a Linkam LTS350. Samples with different wt % and ferrite type were measured during isothermal crystallization at 150, 155, and 160 °C until complete crystallization to study the influence of temperature, ferrite type, and ferrite concentration in the spherulitic growth.

RESULTS

Figure 1 shows the nanocomposite microstructure after 5200 s crystallization time obtained for samples of $CoFe_2O_4$/PVDF with 0.01 wt % of nanoparticles crystallized at different temperatures.

The sample crystallized at 150 °C shows the finest microstructure due to the faster crystallization. With increasing crystallization temperature, the crystallization rate slows down, and the diameter of the spherulites increases.[35] The same behavior was found in the other ferrite/PVDF nanocomposites under investigation (images not shown).

The effect of ferrite concentration in the spherulite microstructure for a given filler concentration is shown in Figure 2 after 5200 s crystallization time for semicrystalline α-PVDF (Figure 2a) and $CoFe_2O_4$/PVDF composites with cobalt ferrite loadings of 0.01 wt % and 1 wt %, respectively (Figure 2b,c) crystallized at 150 °C.

The spherulites of PVDF present in all cases a compact and well-defined microstructure with the Maltese cross-texture typical for PVDF.[32,35] The addition of even the smallest amount of

dx.doi.org/10.1021/jp210493t |J. Phys. Chem. B 2012, 116, 794–801

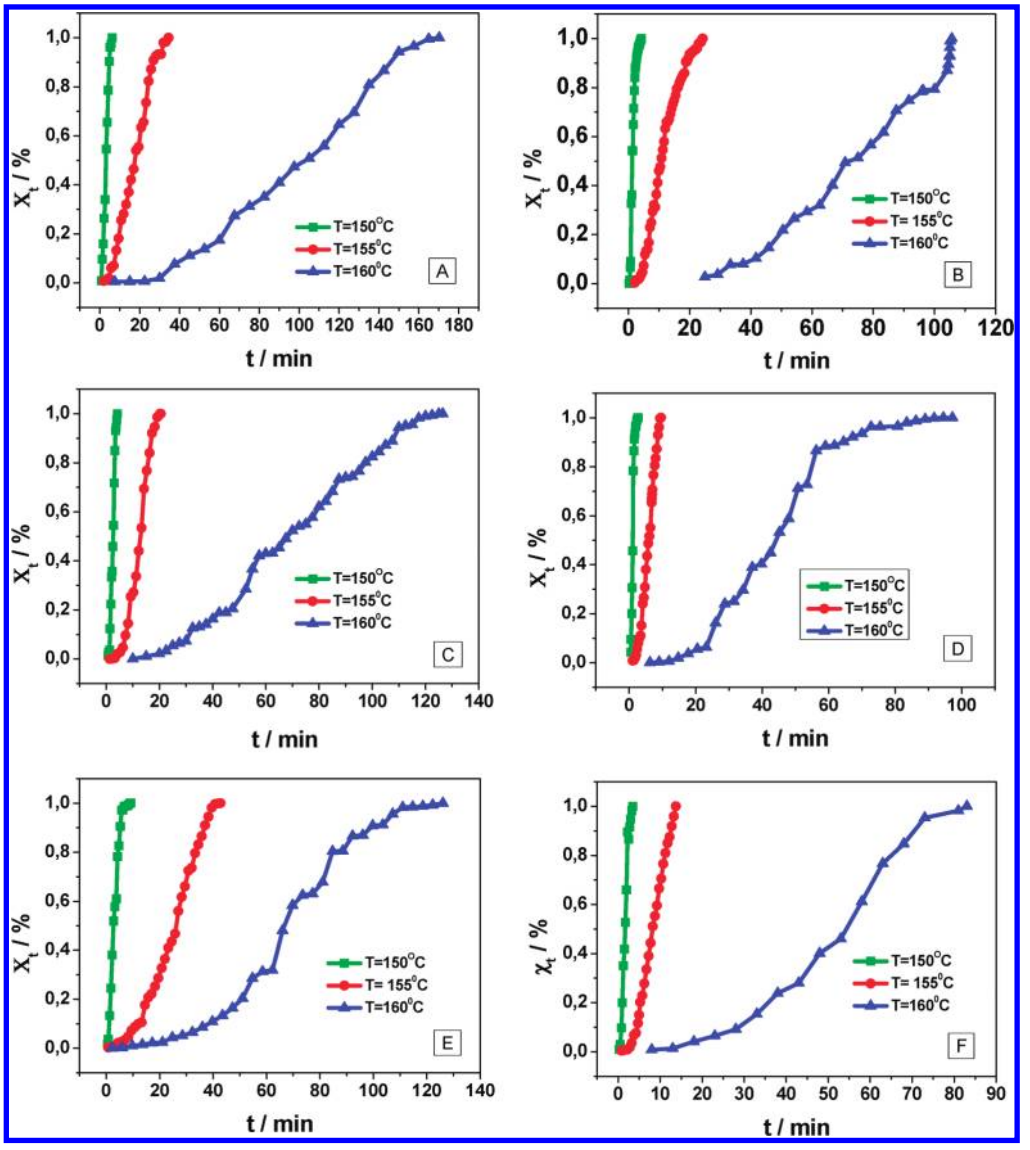

Figure 6. Crystallization isotherms of the ferrite/PVDF nanocomposites for the different crystallization temperatures with (A) α-PVDF, (B) $CoFe_2O_4$/PVDF (0.01 wt %), (C) $CoFe_2O_4$/PVDF (0.5 wt %), (D) $CoFe_2O_4$/PVDF (1 wt %), (E) $Ni_{0.5}Zn_{0.5}Fe_2O_4$/PVDF (0.01 wt %), and (F) $Ni_{0.5}Zn_{0.5}Fe_2O_4$/PVDF (0.01 wt %).

cobalt ferrite nanoparticles increases the number of the spherulites, with the spherulite size decreasing strongly with increasing ferrite concentration for a given crystallization time and temperature (Figure 2b,c). These facts clearly indicate that the nanoparticles effectively act as nucleation agents. With further increasing $CoFe_2O_4$ nanoparticle content, the number of nucleation points grows so much that spherulites cannot be formed. In fact, the sample containing 1 wt % of $CoFe_2O_4$ (Figure 2c) shows almost no definite texture to be observed by polarized light microscopy. Higher particle concentrations turned the samples almost opaque. The results shown in Figure 2 are representative of all three ferrite nanocomposites (not shown).

The spherulitic microstructure of the different nanocomposites ($Ni_{0.5}Zn_{0.5}Fe_2O_4$ /PVDF, $NiFe_2O_4$ /PVDF, and $CoFe_2O_4$/PVDF) with 0.01 wt % nanoparticle content crystallized at 160 °C after 5200 s crystallization time is represented in Figure 3.

The microstructure obtained at 160 °C for the nanocomposite samples indicates that the $NiFe_2O_4$/PVDF nanocomposite (Figure 3b) shows a higher crystallization rate than the $Ni_{0.5}Zn_{0.5}Fe_2O_4$/PVDF and $CoFe_2O_4$/PVDF nanocomposites (Figure 3a,c), once that the final microstructure is already achieved to the $NiFe_2O_4$/PVDF nanocomposite at that crystallization time, contrary to what happens with $Ni_{0.5}Zn_{0.5}Fe_2O_4$/PVDF and $CoFe_2O_4$/PVDF nanocomposites.

As the crystallization rate increases, the PVDF chains change from the β to the α conformation,[39,40] a behavior that is in agreement with previous studies.[20,32] This fact suggests that the crystallization rate in the multiferroic samples and consequently the α-phase nucleation ability follows the order $NiFe_2O_4$/PVDF > $CoFe_2O_4$/PVDF > $Ni_{0.5}Zn_{0.5}Fe_2O_4$/PVDF.

The nucleation ability of the nanoparticles can be quantitatively estimated by the variation of the number of nucleus over time in the samples. This calculation was performed for the composites with 0.01 wt % of ferrite nanoparticles for the three temperatures used in this study (Figure 4). It is observed that the addition of low nanoparticle contents abruptly increases the

dx.doi.org/10.1021/jp210493t |J. Phys. Chem. B 2012, 116, 794–801

number of nuclei comparatively to pure α-PVDF. Further, the nucleation ability is higher in the $Ni_{0.5}Zn_{0.5}Fe_2O_4$ and $CoFe_2O_4$ nanoparticles with respect to $NiFe_2O_4$ ferrite nanoparticles, as corroborated by the larger number of nuclei in the $Ni_{0.5}Zn_{0.5}Fe_2O_4$/PVDF and $CoFe_2O_4$/PVDF nanocomposites. Finally, the increase in the crystallization temperature has a consequence of diminution in the number of nuclei generated, as observed in Figure 4.

DISCUSSION

The crystallization kinetics was studied by analyzing the variation of the radius of the spherulites over time (Figure 5). The data were evaluated during the time in which the spherulites grew independently, with no influence of the neighboring growing spherulites.

For the lowest temperatures, the polymer crystallizes faster, giving rise to the smallest spherulites (Figures 1, 2, and 5). For higher temperatures, the crystallization process is slower, and the diameter of the spherulites is larger.[35]

The addition of $NiFe_2O_4$ and $CoFe_2O_4$ nanoparticles induces the formation of larger spherulites for a given ferrite concentration and crystallization time as compared to the incorporation of $Ni_{0.5}Zn_{0.5}Fe_2O_4$ nanoparticles in the polymer. This result is related to the higher number of nucleus found in the $Ni_{0.5}Zn_{0.5}Fe_2O_4$/PVDF and $CoFe_2O_4$/PVDF nanocomposites. Keeping all other parameters unchanged, a higher number of nuclei implies smaller spherulites.[41]

Plots of the relative crystallinity as a function of time (eq 2) are represented in Figure 6 for different ferrite types, concentrations, and crystallization temperatures. All plots show the typical sigmoidal shape of the isothermal polymer crystallization.[35] Furthermore, the initial slope decreases with increasing crystallization temperature, indicating a progressively slower crystallization rate.[32]

The initial slope is the highest for the $NiFe_2O_4$ nanocomposites and the lowest for the $Ni_{0.5}Zn_{0.5}Fe_2O_4$ samples. This fact confirms that the crystallization rate in the multiferroic samples follows the order $NiFe_2O_4$/PVDF > $CoFe_2O_4$/PVDF > $Ni_{0.5}Zn_{0.5}Fe_2O_4$/PVDF.

After calculation of the relative crystallinity, Figure 7 displays the Avrami plots and respective fittings obtained from eq 5 for the nanocomposites at three different crystallization temperatures.

The plot of

$$\ln[-\ln(1 - X_t)] = \ln K + n \ln t \qquad (5)$$

obtained by linearization of eq 1 produces a straight line with the intercept and slope given by ln K and n, respectively. Typically, the Avrami equation represents correctly only the initial steps of polymer crystallization, characterized by a linear regime.

In the present case, the linear behavior observed indicates that the Avrami equation properly describes the isothermal crystallization behavior of the composite samples. All fittings show a linear fit with $R > 0.99$.

Figure 8a shows the dependence of the Avrami exponent on crystallization temperature. In pure PVDF, a value of n close to 3 is obtained, which indicates that nucleation is heterogeneous and that the growth of spherulites is tridimensional.[42]

With the addition of ferrite nanoparticles, at low crystallization temperatures n decreases by ~1, implying that the nucleation and growth of PVDF becomes two-dimensional.[42]

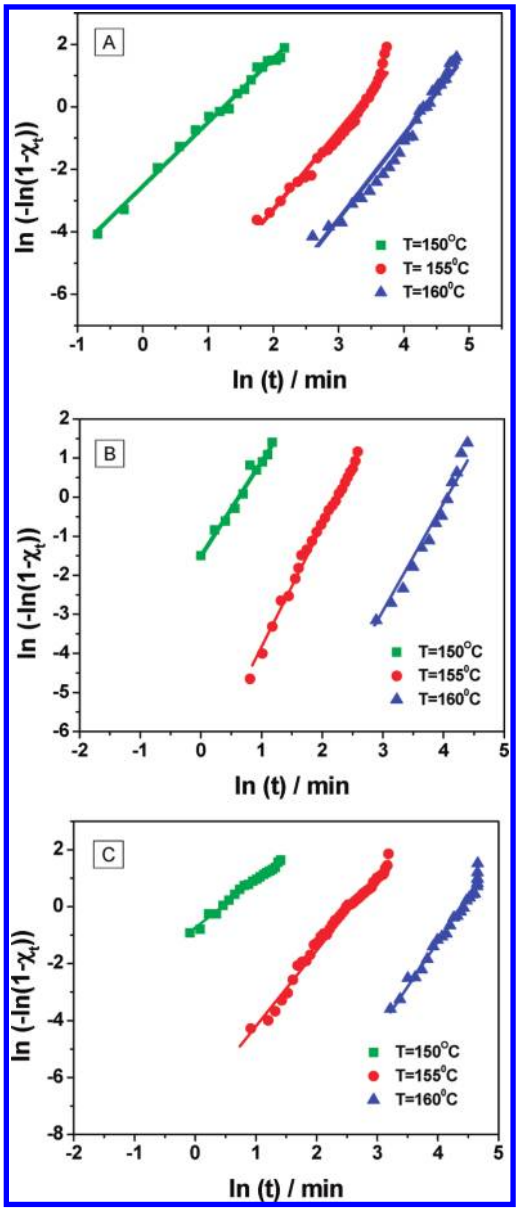

Figure 7. Evolution of the crystallization rate at different temperature of the nanocomposite spherulites with (A) $Ni_{0.5}Zn_{0.5}Fe_2O_4$, (B) $NiFe_2O_4$, and (C) $CoFe_2O_4$ nanoparticles.

The temperature dependence of the Avrami exponent in the same type of nanocomposites with higher loadings of ferrite nanoparticles has been recently reported, being approximately equal to that obtained for the α-PVDF sample[32]

Figure 8b shows the evolution of the induction time, defined as the period needed to form a critical nucleus during which no crystallinity is observed,[43] for the pure polymer and for the ferrite nanocomposite samples as a function of the crystallization temperature. A decrease in the induction time is observed with increasing ferrite wt %, being this decrease more significant for the higher crystallization temperatures. The decrease of the induction time is associated to the nucleation rate, which is controlled by the availability and the concentration of the heterogeneous nuclei. As a result, ferrite nanoparticles in the polymeric matrix serve as heterogeneous nucleating sites and are more effective at higher temperatures due to the slower crystallization.[44]

dx.doi.org/10.1021/jp210493t |J. Phys. Chem. B 2012, 116, 794–801

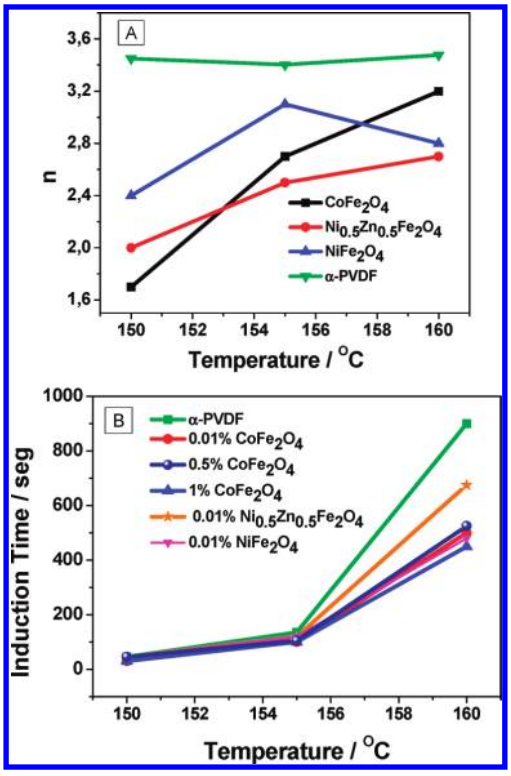

Figure 8. (A) Evolution of the Avrami exponent with the crystallization temperature of ferrite/PVDF (0.01 wt %). (B) Half-time of the crystallization as a function of the crystallization temperature.

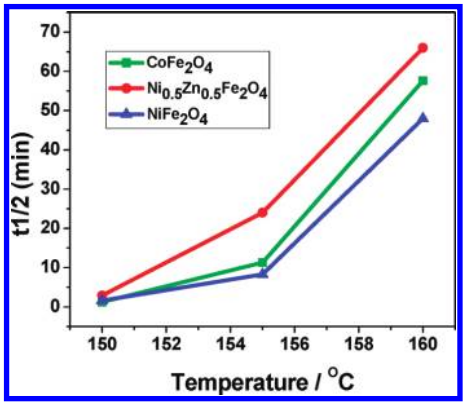

Figure 9. Crystallization half-time $t_{1/2}$ vs crystallization temperature to ferrite/PVDF (0.01 wt.%) nanocomposites.

The decrease in the induction time with respect to the polymer matrix follows the order $Ni_{0.5}Zn_{0.5}Fe_2O_4$/PVDF > $CoFe_2O_4$/PVDF > $NiFe_2O_4$ /PVDF.

For a pure polymer melt, the nucleation step involves the folding of polymer chains and the formation of solid surfaces that become the nuclei for crystallization;[45] the energy barrier for this process is usually very high. The existence of a foreign solid surface such as ferrite nanoparticles in the melt, as observed, anticipates the nucleation step.[45]

The $t_{1/2}$ evolution with the crystallization temperature, calculated by eq 3, for the samples with 0.01 wt % of ferrite content is represented in Figure 9. As expected, the crystallization half-time increases with increasing crystallization temperature.

Table 1. Avrami Parameters Obtained from the Fittings with eqs 1 and 4, Describing the Crystallization Kinetic of PVDF Nanocomposites upon Isothermal Crystallization from the Melt

nanocomposite	temp (°C)	n	K (min)	$t_{1/2}$ (min)	E_{act} (kJ mol^{-1})
0.01% $CoFe_2O_4$	150	1.7	0.48	1.24	1.309
	155	2.7	0.001	11.28	
	160	3.2	8.87×10^{-7}	58	
0.01% $NiZnFe_2O_4$	150	2	0.08	2.9	1.392
	155	2.5	2.44×10^{-4}	24	
	160	2.7	8.60×10^{-6}	66	
0.01% $NiFe_2O_4$	150	2.4	0.22	1.6	1.473
	155	3.1	9.76×10^{-4}	8.3	
	160	2.8	1.38×10^{-5}	48	
0.5% $CoFe_2O_4$	150	3.5	0.03	2.5	1.509
	155	3.98	3.10×10^{-5}	12	
	160	3.1	1.50×10^{-6}	67	
1% $CoFe_2O_4$	150	2.93	0.49	1.12	1.838
	155	2.95	4.04×10^{-3}	5.72	
	160	3.3	2.76×10^{-6}	43	
α-PVDF	150	2.46	0.046	3	1.389
	155	2.36	8.81×10^{-4}	17	
	160	2.6	4.96×10^{-6}	95	

Table 1 summarizes the crystallization parameters for the isothermal crystallization of PVDF and nanocomposites obtained from the fittings with eqs 1 and 5.

Although the incorporation of ferrite nanoparticles can induce heterogeneous nucleation and accelerate the isothermal crystallization of PVDF nanocomposites, nanoparticles may also restrict the movement of polymer chains, thereby making crystallization more difficult. The values of the crystallization activation energy are the combined results of the above two competing effects of nucleation and restriction.[46] The obtained value for the α-PVDF activation energy is in the same order of previous investigations.[47,48] Fine dispersion in the nanocomposite with 0.01 wt % of $CoFe_2O_4$ was achieved, and the nucleating effect of nanoparticles was most significant; thus, its crystallization activation energy was the lowest. The increasing crystallization activation energy with increasing ferrite content results from the restriction of polymer chain movements caused by high ferrite loading.[46]

In this way, additionally to previous investigations,[32] the crystallization behavior of the composite samples presented in this study and the obtained Avrami parameters show the higher nucleation ability and the lower crystallization velocity of the $Ni_{0.5}Zn_{0.5}Fe_2O_4$ and $CoFe_2O_4$ nanocomposites with respect to $NiFe_2O_4$ nanocomposites. This is in agreement with the PVDF β-phase nucleation ability of those three ferrites.[20]

CONCLUSIONS

The isothermal crystallization behavior from the melt and the growth kinetics of neat PVDF and ferrite nanocomposites were studied by polarized optical microscopy. The results indicated that the addition of ferrite nanoparticles leads to an increase of the nucleation kinetics of PVDF, which is ascribed to the nucleating effect of ferrite nanoparticles. The incorporation of

dx.doi.org/10.1021/jp210493t |J. Phys. Chem. B 2012, 116, 794–801

ferrite nanoparticles increases the number of spherulites and thus decreases significantly the spherulite size of PVDF. The nucleation ability is higher for the $Ni_{0.5}Zn_{0.5}Fe_2O_4$ and $CoFe_2O_4$ nanoparticles with respect to $NiFe_2O_4$ nanoparticles, and the crystallization rate in the multiferroic samples was found to follow the order $NiFe_2O_4$/PVDF > $CoFe_2O_4$/PVDF > $Ni_{0.5}Zn_{0.5}Fe_2O_4$/PVDF. Higher activation energies of the nanocomposites with respect to that of neat PVDF can be attributed to the movement restriction of polymer chains caused by the presence of ferrite nanoparticles. In this way, the crystallization behavior of the composite samples presented in this study and the obtained Avrami show the higher nucleation ability and the lower crystallization velocity of the $Ni_{0.5}Zn_{0.5}Fe_2O_4$ and $CoFe_2O_4$ nanocomposites with respect to $NiFe_2O_4$ nanocomposites, which in turns results in a larger ability for the nucleation of the PVDF β-phase of those ferrite fillers.

AUTHOR INFORMATION

Corresponding Author

*E-mail: lanceros@fisica.uminho.pt.

ACKNOWLEDGMENT

We acknowledge the Foundation for Science and Technology (FCT) for finantial support through PTDC/CTM/69316/2006, PTDC/CTM-NAN/112574/2009, and NANO/NMed-SD/0156/2007 projects. P.M. and C.M.C. thank the support of the FCT (grant SFRH/BD/45265/2008 and SFRH/BD/68499/2010). We also thank the support from the COST Action MP1003, 2010 'European Scientific Network for Artificial Muscles'.

REFERENCES

(1) Broadhurst, M. G.; Davis, G. T. *Ferroelectrics* **1984**, *60*, 3–13.
(2) Murayama, N.; Nakamura, K.; Obara, H.; Segawa, M. *Ultrasonics* **1976**, *14*, 15–23.
(3) Lanceros-Mendez, S.; Mano, J. F.; Costa, A. M.; Schmidt, V. H. *J. Macromol. Sci., Part B: Phys.* **2001**, *B40*, 517–527.
(4) Gregorio, R.; Cestari, M.; Chaves, N. *The Polymeric Material Encyclopedia*;CRC Press: Boca Raton, FL, 1996.
(5) Kang, S. J.; Park, Y. J.; Hwang, J.; Jeong, H. J.; Lee, J. S.; Kim, K. J.; Kim, H. C.; Huh, J.; Park, C. *Adv. Mater.* **2007**, *19*, 581–+.
(6) Lovinger, A. J. *Science* **1983**, *220*, 1115–1121.
(7) Sencadas, V.; Gregorio, R.; Lanceros-Mendez, S. *J. Non-Cryst. Solids* **2006**, *352*, 2226–2229.
(8) Martins, P.; Nunes, J. S.; Hungerford, G.; Miranda, D.; Ferreira, A.; Sencadas, V.; Lanceros-Mendez, S. *Phys. Lett. A* **2009**, *373*, 177–180.
(9) Fukada, E. *IEEE Trans. Ultrason. Ferroelectr. Freq. Contr.* **2000**, *47*, 1277–1290.
(10) He, L.; Xu, Q.; Hua, C.; Song, R. *Polym. Compos.* **2010**, *31*, 921–927.
(11) Ribeiro, C.; Sencadas, V.; Ribelles, J. L. G.; Lanceros-Mendez, S. *Soft Mater.* **2010**, *8*, 274–287.
(12) Magalhaes, R.; Duraes, N.; Silva, M.; Silva, J.; Sencadas, V.; Botelho, G.; Ribelles, J. L. G.; Lanceros-Mendez, S. *Soft Mater.* **2011**, *9*, 1–14.
(13) Jiang, Z.; Carroll, B.; Abraham, K. M. *Electrochim. Acta* **1997**, *42*, 2667–2677.
(14) Ferreira, A.; Costa, P.; Carvalho, H.; Nobrega, J.; Sencadas, V.; Lanceros-Mendez, S. *J. Polym. Res.* **2011**, *18*, 1653–1658.
(15) Sencadas, V.; Gregorio, R.; Lanceros-Méndez, S. *J. Macromol. Sci., Part B: Phys.* **2009**, *48*, 514–525.
(16) Priya, L.; Jog, J. P. *J. Polym. Sci., Part B: Polym. Phys.* **2002**, *40*, 1682–1689.
(17) Sadeghi, F.; Ajji, A. *Polym. Eng. Sci.* **2009**, *49*, 200–207.
(18) Lopes, A. C.; Costa, C. M.; Tavares, C. J.; Neves, I. C.; Lanceros-Mendez, S. *J. Phys. Chem. C* **2011**, *115*, 18076–18082.
(19) Andrew, J. S.; Clarke, D. R. *Langmuir* **2008**, *24*, 8435–8438.
(20) Martins, P.; Costa, C. M.; Lanceros-Mendez, S. *Appl. Phys. A* **2011**, *103*, 233–237.
(21) Martins, P.; Moya, X.; Phillips, L. C.; Kar-Narayan, S.; Mathur, N. D.; Lanceros-Mendez, S. *J. Phys. D: Appl. Phys.* **2011**, *44*, 482001.
(22) Ramesh, R.; Spaldin, N. A. *Nat. Mater.* **2007**, *6*, 21–29.
(23) Dillon, D. R.; Tenneti, K. K.; Li, C. Y.; Ko, F. K.; Sics, I.; Hsiao, B. S. *Polymer* **2006**, *47*, 1678–1688.
(24) Mago, G.; Fisher, F. T.; Kalyon, D. M. *J. Nanosci. Nanotechnol.* **2009**, *9*, 3330–3340.
(25) Xu, W. B.; Ge, M. L.; He, P. S. *J. Polym. Sci., Part B: Polym. Phys.* **2002**, *40*, 408–414.
(26) Qian, J. S.; He, P. S. *J. Mater. Sci.* **2003**, *38*, 2299–2304.
(27) Kim, S. H.; Ahn, S. H.; Hirai, T. *Polymer* **2003**, *44*, 5625–5634.
(28) Achilias, D. S.; Bikiaris, D. N.; Papastergiadis, E.; Giliopoulos, D.; Papageorgiou, G. Z. *Macromol. Chem. Phys.* **2010**, *211*, 66–79.
(29) Naffakh, M.; Marco, C.; Gomez, M. A.; Jimenez, I. *Mater. Chem. Phys.* **2011**, *128*, 265–273.
(30) Kim, G. H.; Hong, S. M.; Seo, Y. *Phys. Chem. Chem. Phys.* **2009**, *11*, 10506–10512.
(31) Manna, S.; Batabyal, S. K.; Nandi, A. K. *J. Phys. Chem. B* **2006**, *110*, 12318–12326.
(32) Sencadas, V.; Martins, P.; Pitães, A.; Benelmekki, M.; Gómez Ribelles, J. L.; Lanceros-Mendez, S. *Langmuir* **2011**, *27*, 7241–7249.
(33) Avrami, M. *J. Chem. Phys.* **1939**, *7*, 1103–1112.
(34) Avrami, M. *J. Chem. Phys.* **1941**, *9*, 177–184.
(35) Silva, M. P.; Sencadas, V.; Botelho, G.; Machado, A. V.; Rolo, A. G.; Rocha, J. G.; Lanceros-Mendez, S. *Mater. Chem. Phys.* **2010**, *122*, 87–92.
(36) Long, Y.; Shanks, R. A.; Stachurski, Z. H. *Prog. Polym. Sci.* **1995**, *20*, 651–701.
(37) Qiu, Z. B.; Yan, C. Z.; Lu, J. M.; Yang, W. T. *Macromolecules* **2007**, *40*, 5047–5053.
(38) Martins, P.; Costa, C. M.; Benelmekki, M.; Botelho, G.; Lanceros-Mendez, S. *CrystEngComm* **2012**, to be published.
(39) Cebe, P.; Chung, S. Y. *J. Mater. Sci.* **1990**, *25*, 2367–2378.
(40) Lee, J. G.; Kim, S. H. *Macromol. Res.* **2011**, *19*, 72–78.
(41) Tanniru, M.; Misra, R. D. K.; Berbrand, K.; Murphy, D. *Mater. Sci. Eng., A* **2005**, *404*, 208–220.
(42) Liu, Z. H.; Marechal, P.; Jerome, R. *Polymer* **1997**, *38*, 5149–5153.
(43) Mamun, A.; Umemoto, S.; Ishihara, N.; Okui, N. *Polymer* **2006**, *47*, 5531–5537.
(44) Chae, D. W.; Hong, S. M. *J. Polym. Sci., Part B: Polym. Phys.* **2010**, *48*, 2379–2385.
(45) Xu, L.; Weiss, R. A. *Macromolecules* **2003**, *36*, 9075–9084.
(46) Chen, D.; Wu, M.; Wang, W. Z.; Liu, T. X. *J. Macromol. Sci., Part B: Phys.* **2010**, *49*, 1069–1082.
(47) Elashmawi, I. S.; Elsheshtawi, N. A.; Abdelkader, H. I.; Hakeem, N. A. *Cryst. Res. Technol.* **2007**, *42*, 157–163.
(48) Asai, K.; Okamoto, M.; Tashiro, K. *Polymer* **2008**, *49*, 5186–5190.